Multiresolution spline-based 3D/2D registration of CT volume and C-arm images for computer-assisted surgery

Slavica Jonić, Philippe Thévenaz, Michael Unser

Swiss Federal Institute of Technology Lausanne, CH–1015 Lausanne EPFL, Switzerland

ABSTRACT

We propose an algorithm for aligning a preoperative computed tomography (CT) volume and intraoperative C-arm images, with applications in computer-assisted spinal surgery. Our three-dimensional (3D)/two-dimensional (2D) registration algorithm is based on splines and is tuned to a multiresolution strategy. Its goal is to establish the mutual relations of locations in the real-world scene to locations in the 3D CT and in the 2D C-arm images. The principle of the solution is to simulate a series of C-arm images, using CT data only. Each numerical simulation of a C-arm image is defined by its pose. Our registration algorithm then adjusts this pose until the given C-arm projections and the simulated projections exhibit the greatest degree of similarity. We show the performance of the algorithm for the experiments in a controlled environment which allows for an objective validation of the quality of our algorithm. For each of 100 randomly generated disturbances around the optimum solution, the 3D/2D registration algorithm was successful and resulted in image registration with subpixel error.

Keywords: Computer-assisted surgery, spinal surgery, image-guided surgery, 3D/2D image registration, voxel-based registration, splines, multiresolution

1. INTRODUCTION

This paper proposes an algorithm for the accurate registration of three-dimensional (3D) to two-dimensional (2D) data, with applications in computer-assisted spinal surgery. We focus on the registration of a preoperative CT volume with intraoperative C-arm images of the spine, which is particularly relevant for guiding the procedure of spinal fixation by transpedicular screws.[1,2]

The accuracy of registration is a crucial aspect of our work. Surgeons and physicians plan the intervention on the basis of the preoperative CT data, and rely on the intraoperative C-arm images to navigate their tools around and inside the patient. Thus, while registering preoperative to intraoperative data, one has to bear in mind the dire consequences of inaccurate registration. Meanwhile, a successful registration will allow for the most efficient use of the preoperative planning. In combination with an optical tracking device, it will also allow for the integration and the interactive display of tools over the CT and C-arm images, in real-time.

We reach accuracy through a careful design of all registration components. Perhaps the most important of them is the interpolation model which specifies how one should resample the available discrete data so as to modify their position or orientation in space. In the present case, we have selected a continuous image model that is based on cubic splines[3–5] and that is tuned to a multiresolution strategy.[6,7] By opposition to several other algorithms available in the literature which are based on nearest-neighbor or linear interpolation, we choose cubic spline interpolation because of its better order of approximation. This model provides a good compromise between the aliasing which dominates for low degrees and the ringing present for higher degrees.

The benefits of using a high-quality interpolation model are threefold. First, our 2D computed projections are accurate thanks to its high order of approximation. Second, it allows for the exact computation of gradients, as opposed to their estimation: often, we observe that other researchers perform optimization with approximate gradients instead. The fact that our gradient computations are exact promotes accuracy. Third, the rescaled

Further author information: (Send correspondence to S.J.)
S.J.: E-mail: slavica.jonic@epfl.ch
P.T.: E-mail: philippe.thevenaz@epfl.ch
M.U.: E-mail: michael.unser@epfl.ch
URL: http://bigwww.epfl.ch/

versions of our interpolation model yield a spline-based image pyramid for a multiresolution approach. This results in more robust registration.

Feature-based 3D/2D registration is based on the identification of characteristic features present in each of the two images, which requires segmentation.[8–10] Once the features are available, the registration is usually fast; a major drawback is the high dependence of the registration accuracy on the accuracy of the segmentation itself, which is notorious for being difficult to achieve. By contrast, voxel-based methods require neither data interpretation nor segmentation.[11–15]

They compare the voxel values of a 3D image with the pixel values of a 2D image directly, using a measure based on image statistics. Generally, these methods are slower but more accurate and more robust. Since a major goal of this paper is to obtain high registration accuracy, we will focus on a voxel-based method.

All voxel-based 3D/2D registration algorithms must address the three following questions: 1) Which measure of similarity to adopt between the 3D data and the 2D projections? 2) How to obtain simulated projections out of the volumetric data in order to compare them with the given C-arm projections? and 3) How to optimize the measure of similarity?

To answer the first question, we remark that both the C-arm devices and the CT scanner are built upon the same physical principle: both rely on x-rays to probe the patient. Thus, a natural idea is to simulate C-arm images from the CT data, and to adjust the pose of the simulated C-arm devices until they produce images that are similar to the given ones—for which the true pose is known thanks to a tracking device. To obtain a simulated C-arm projection, we simply integrate the CT volume along the direction of the simulated x-ray*. We then select our measure of similarity as the mean-square difference between a simulated projection and a given one.

To answer the second question in the context of intraoperative applications, we remark that it is highly desirable that the registration be performed in a few seconds. Since a large fraction of the processing effort is devoted to the computation of 2D projections from 3D data, great efforts have been made to discover fast methods without compromising the quality.[11–15] We propose here a new projection method that we call *projective integration*. By carefully controlling the step of a Riemann sum, we need only 2D interpolation to project 3D data along any direction. This approach is related to the shear-warp factorization of a transformation, but avoids to have to interpolate data twice to obtain a projection.[15]

The third question regards the selection of the optimizer. In this paper, we use the Marquardt-Levenberg non-linear least-squares optimizer.[16] This optimizer is particularly well adapted to a multiresolution context because at any level it can refine in just a few steps the best solution found at a coarser level. It achieves efficiency by considering all optimization parameters in parallel, as opposed to other optimizers that perform sequential optimization instead.[15] A further benefit of multiresolution is increased registration robustness. In this paper nevertheless, we will present the registration algorithm out of the multiresolution context.

2. BUILDING BRICKS

2.1. Image Model

To interpolate accurately the CT volume data when simulating C-arm images, we use a continuous image model based on splines.[3–5] This model is given by

$$f(\mathbf{x}) = \sum_{\mathbf{i} \in \mathbb{Z}^N} c_{\mathbf{i}} \, \beta^n(\mathbf{x} - \mathbf{i}),$$

where $\beta^n(\mathbf{x})$ is a separable convolution kernel which is, in the N-dimensional case, given by the product

$$\beta^n(\mathbf{x}) = \prod_{j=1}^{N} \beta^n(x_j),$$

and where the coefficients $c_{\mathbf{i}}$ are precomputed from the given data samples $f(\mathbf{i})$ by recursive digital filtering.[4]

*In this paper, we disregard x-ray attenuation and we consider the simplified case of a parallel instead of a conical beam.

The model degree n determines the interpolation quality which affects the precision of the registration. The spatial gradient of the image is given by

$$\boldsymbol{\nabla} f(\mathbf{x}) = \sum_{\mathbf{i} \in \mathbb{Z}^N} c_{\mathbf{i}} \, \boldsymbol{\nabla} \beta^n(\mathbf{x} - \mathbf{i}).$$

For $2 \leq n$, we have the guarantee that $\boldsymbol{\nabla} \beta^n(\mathbf{x})$ is continuous and that the derivatives are well defined everywhere, which is clearly not the case with the piecewise-constant or the linear model used in most implementations. An additional advantage of using a B-spline image model is in yielding a spline-based image pyramid for a multiresolution approach which is recommended for a fast and robust registration.

2.2. Simulated C-Arm Image

To align a CT volume with a set of 2D C-arm images, we have to compare the given C-arm images with simulated projections obtained by integrating the volumetric data. We describe the pose $\boldsymbol{\mu} = ((\phi, \theta), \psi; \boldsymbol{\delta})$ of a simulated C-arm image $\mathbb{P}$ by a unit vector $\mathbf{c}$ in spherical coordinates $(1, \phi, \theta)$ that is perpendicular to the projection plane. The pose description is completed by a rotation angle ψ around the axis defined by $\mathbf{c}$, and by a translation $\boldsymbol{\delta} = (\delta_1, \delta_2, \delta_3)$ in Cartesian coordinates. For any $\mathbf{x} \in \mathbb{P}$, we write the projection $p_{3\mathrm{D}}(\boldsymbol{\mu}, f)$ of a volume f and for the pose $\boldsymbol{\mu}$ as

$$p_{3\mathrm{D}}(\mathbf{x}; \boldsymbol{\mu}, f) = \int_{-\infty}^{\infty} f(\mathbf{x} - \boldsymbol{\delta} + t \, \mathbf{c}) \, \mathrm{d}t.$$

To map the projection plane $\mathbb{P}$ into a set of scanning 2D coordinates (or indexes) of homogenous coordinates $\mathbf{k} = (k_1, k_2, 0, 1)$, we express the matrix B (that solely depends on $\boldsymbol{\mu}$) such that $\forall (k_1, k_2) \in \mathbb{R}^2 : \; B \, \mathbf{k} \in \mathbb{P}$. Finally, the simulated C-arm image $p(\boldsymbol{\mu}, f)$ with the pose $\boldsymbol{\mu}$, using the CT volume f, is given by

$$p(\mathbf{k}; \boldsymbol{\mu}, f) = \int_{-\infty}^{\infty} f(B \, \mathbf{k} + t \, \mathbf{c}) \, \mathrm{d}t. \tag{1}$$

2.3. Projective Integration

A direct implementation of Equation (1) would require the interpolation of 3D data samples. Here instead, we propose an alternative that reduces the computational demands by performing 2D interpolation. The principle is to approximate the integral in Equation (1) by a Riemann sum and to adapt the sampling step such that only samples with integer argument take part in the sum. We proceed by performing the following change of the variable t:

$$t = \frac{\xi_j - [B \, \mathbf{k}]_j}{[\mathbf{c}]_j}, \; \mathrm{d}t = \frac{1}{[\mathbf{c}]_j} \, \mathrm{d}\xi_j. \tag{2}$$

where ξ_j, $j \in \{1, 2, 3\}$ are the new variables, and where $[x]_j$ indicates the j-th component of the vector $\mathbf{x}$. After introducing Equation (2) in (1), we get that

$$p(\mathbf{k}; \boldsymbol{\mu}, f) = \frac{1}{[\mathbf{c}]_j} \int_{-\infty}^{\infty} f(B \, \mathbf{k} + (\xi_j - [B \, \mathbf{k}]_j) \, \frac{\mathbf{c}}{[\mathbf{c}]_j}) \, \mathrm{d}\xi_j. \tag{3}$$

Since $[B \, \mathbf{k} + (\xi_j - [B \, \mathbf{k}]_j) \, \mathbf{c}/[\mathbf{c}]_j]_j = \xi_j$, it is obvious that the integration is performed along the j-th major axis of f. Then, we use the Riemann-sum approximation of the integral where the continuous integration variable ξ_j in Equation (3) is replaced by a discrete index n_j. From $[B \, \mathbf{k} + (n_j - [B \, \mathbf{k}]_j) \, \mathbf{c}/[\mathbf{c}]_j]_j = n_j$ follows that the j-th component of the vector of coordinates of the volume f is always integer, which results in

$$p(\mathbf{k}; \boldsymbol{\mu}, f) \approx \frac{1}{[\mathbf{c}]_j} \sum_{n_j \in \mathbb{Z}} f(B \, \mathbf{k} + (n_j - [B \, \mathbf{k}]_j) \, \frac{\mathbf{c}}{[\mathbf{c}]_j}).$$

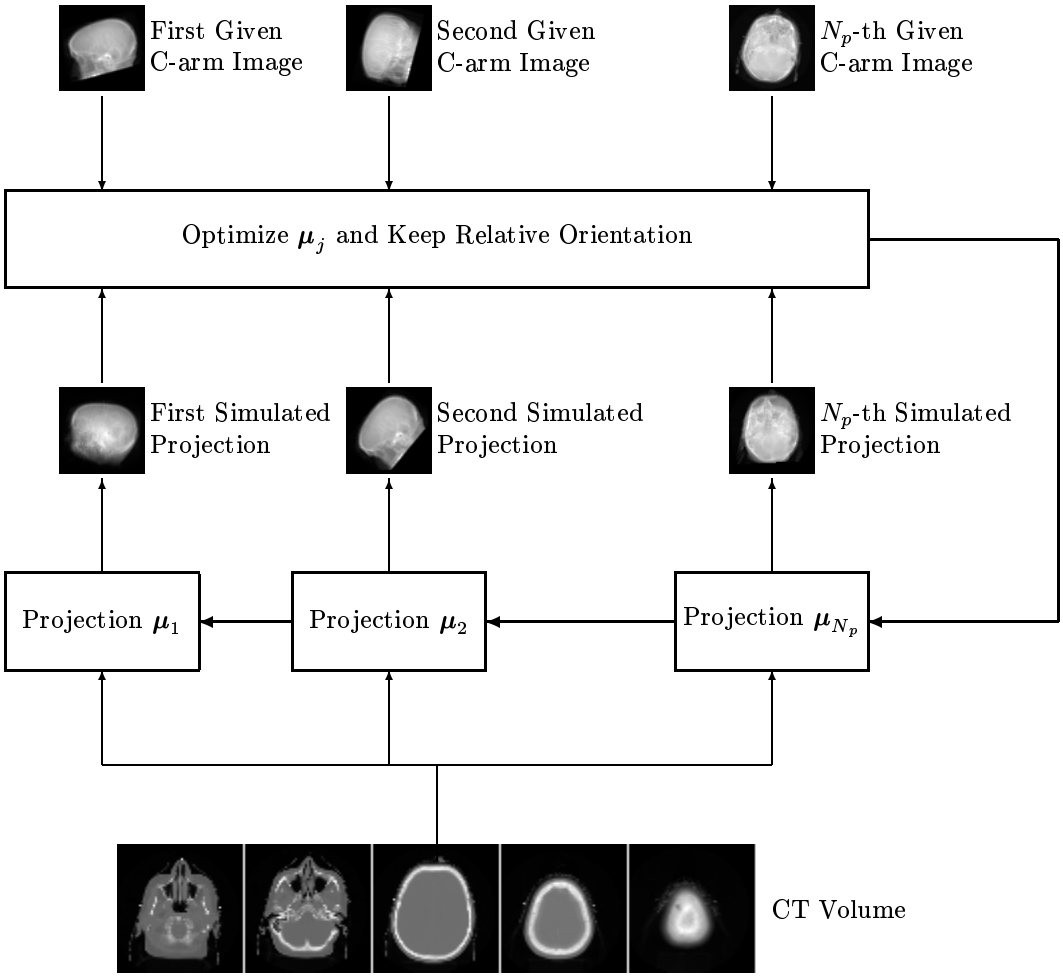

Figure 1. Diagram of the 3D/2D registration algorithm

3. REGISTRATION ALGORITHM

3.1. Principle

Figure 1 shows the block-diagram of our registration algorithm. The input data for the algorithm are: 1) a CT volume, 2) a number of C-arm images that correspond to different projection orientations, and 3) the absolute pose of the C-arm images given in tracking-device coordinates, out of which we deduce their relative pose.

The registration algorithm proceeds in the space of CT coordinates. In this space, the pose of the CT volume is fixed, while the pose $\boldsymbol{\mu}_j$ of the j-th simulated C-arm image is unknown and must be recovered $\forall j \in \{1 \dots N_p\}$, where N_p gives the number of views. Because we ensure that the simulated C-arm devices maintain their relative pose during the whole registration process, it is enough to recover one simulated pose to recover them all—note that at least two imaging views are necessary. We tune the parameters $\boldsymbol{\mu}$ until the given and simulated C-arm images reach the greatest degree of similarity for all imaging views.

3.2. Optimization

3.2.1. Criterion

Our measure of similarity between the given and the simulated projections is the mean-square criterion given by

$$S(\boldsymbol{\mu}) = \frac{1}{2} \sum_{j=1}^{N_p} \frac{1}{\mathrm{card}(\mathbb{D}_j)} \sum_{\mathbf{k} \in \mathbb{D}_j} \left(p(\mathbf{k}; \boldsymbol{\mu}_j, f) - p_j(\mathbf{k}) \right)^2,$$

where $p(\boldsymbol{\mu}_j, f)$ is the j-th simulated C-arm image for the pose $\boldsymbol{\mu}_j$, computed by projective integration of the volume f, and where p_j is the j-th given C-arm image. The domain $\mathbb{D}_j$ corresponds to an arbitrary mask. In practice, this mask is determined by the overlap of the projections.

3.2.2. Gradient and Hessian

The gradient $\boldsymbol{\nabla} S$ is the six-component vector of the first derivatives of the criterion $S(\boldsymbol{\mu})$ with respect to the parameters $\boldsymbol{\mu}$. It is given by

$$\boldsymbol{\nabla} S = \left(\frac{\partial S}{\partial \mu_1}, \frac{\partial S}{\partial \mu_2}, \ldots, \frac{\partial S}{\partial \mu_6} \right).$$

The Hessian $\Delta^2 S$ is the six-by-six matrix of the second derivatives of $S(\boldsymbol{\mu})$ with respect to the parameters $\boldsymbol{\mu}$. It is given by

$$\Delta^2 S = \begin{pmatrix} \frac{\partial^2 S}{\partial \mu_1 \partial \mu_1} & \frac{\partial^2 S}{\partial \mu_1 \partial \mu_2} & \cdots \\ \frac{\partial^2 S}{\partial \mu_2 \partial \mu_1} & \frac{\partial^2 S}{\partial \mu_2 \partial \mu_2} & \cdots \\ \vdots & \vdots & \ddots \end{pmatrix}.$$

The exact components of the Hessian matrix depend on the first derivatives of the simulated C-arm images $p(\boldsymbol{\mu}_j, f)$ with respect to the parameters $\boldsymbol{\mu}$ as well as on their second derivatives. Because the influence of the second derivative terms can be destabilizing, we use the following approximation of the elements of the Hessian matrix which ignores them[17]:

$$\frac{\partial^2 S}{\partial \mu_l \, \partial \mu_m} \approx \sum_{j=1}^{N_p} \frac{1}{\mathrm{card}(\mathbb{D}_j)} \sum_{\mathbf{k} \in \mathbb{D}_j} \frac{\partial p(\mathbf{k}; \boldsymbol{\mu}_j, f)}{\partial \mu_l} \frac{\partial p(\mathbf{k}; \boldsymbol{\mu}_j, f)}{\partial \mu_m}.$$

The use of such an approximation has two positive effects. It makes the optimization work better because 1) it provides a Hessian matrix that is positive definite, and because 2) it reduces the destabilizing effects of the second derivatives when the current guess is far from the solution.

3.2.3. Marquardt-Levenberg optimizer

Let H be a modified Hessian such that the diagonal elements of the true Hessian $\Delta^2 S$ are multiplied by a factor λ while its off-diagonal elements are not changed. It is thus given by

$$[H(\boldsymbol{\mu})]_{i,j} = [\Delta^2 S(\boldsymbol{\mu})]_{i,j} \, (1 + \lambda \, \delta_{i,j}),$$

where $\delta_{i,j}$ is the Kronecker symbol and $i, j \in \{1, 2, \ldots, 6\}$. Then, the Marquardt-Levenberg optimization algorithm can be described by[16]

$$\boldsymbol{\mu}^{(k+1)} = \boldsymbol{\mu}^{(k)} - (H(\boldsymbol{\mu}^{(k)}))^{-1} \, \boldsymbol{\nabla} S(\boldsymbol{\mu}^{(k)}), \tag{4}$$

where $\boldsymbol{\mu}^{(k)}$ are the parameters $\boldsymbol{\mu}$ at the iteration k, and where $\boldsymbol{\mu}^{(k+1)}$ is their update for the iteration $(k+1)$. When $\lambda \to +\infty$, Equation (4) approximates the gradient algorithm which is robust but generally inefficient. When $\lambda \to 0$, Equation (4) approximates the Newton algorithm which is efficient but not robust. The parameter λ is a factor which has to be tuned so that the best compromise between the Newton method and the gradient method is achieved.

4. EXPERIMENTS

4.1. Methodology

We show the performance of our algorithm in a case where the true alignment is known *a priori*. This controlled environment allows for an objective validation of the quality of our algorithm. We perform this validation study by using the geometric error of Section 4.2 as figure of merit.

The most convenient way to have a complete and precise control over the geometric aspects of the experiment is that the given C-arm images be obtained in the same fashion as we obtain the simulated ones. Therefore, we use the results of Section 2.3 for both cases, up to the following detail: if we project the same volume data to compute given and simulated C-arm images, then we are potentially able to achieve perfect registration. To make the situation less ideal, we apply a known rigid-body geometric transformation $\mathbf{g}(\boldsymbol{\mu}_0)$ to the given volume f, which

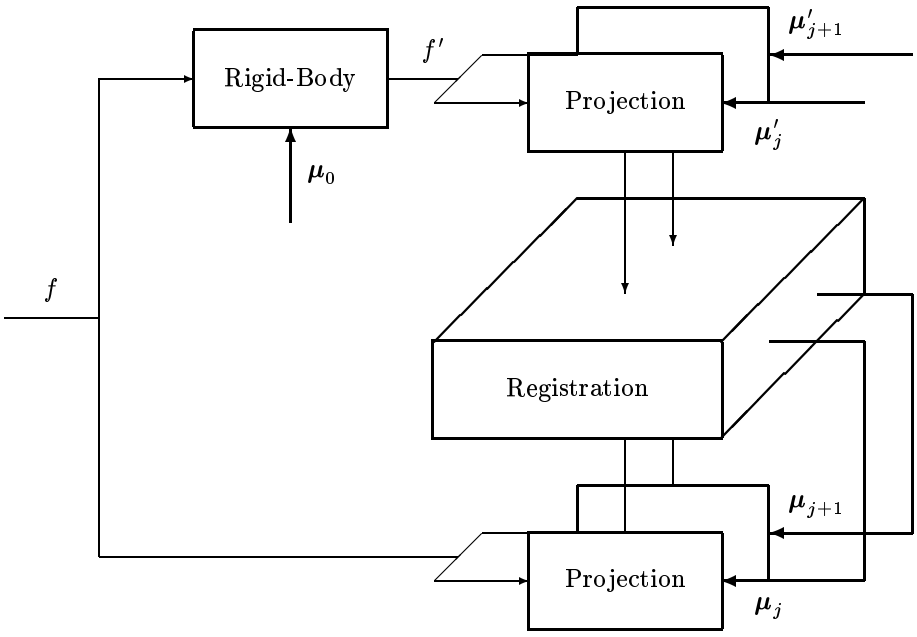

Figure 2. Diagram of the test procedure. Because of interpolation and clipping, there exists no set of parameters $\boldsymbol{\mu}$ such that a projection of f is exactly identical to a projection of f'.

results in $f'(\mathbf{k}) = f(\mathbf{g}(\mathbf{k}; \boldsymbol{\mu}_0))$. This operation introduces interpolation and clipping, which ensures that it is not possible anymore to find registration parameters $\boldsymbol{\mu}$ such that $S(\boldsymbol{\mu}) = 0$. Figure 2 depicts the general procedure.

The goal of the registration is to find a set of poses $\boldsymbol{\mu}_j$, $j \in \{1, \ldots, N_p\}$, for which the simulated C-arm images are the most similar to the given ones, on average. Since we maintain at all times the relative orientation of the C-arms, one element of the set is enough to describe the whole set. Thus, let us denote by $\tilde{\boldsymbol{\mu}}$ the pose estimate found by the registration algorithm. It follows that the best alignment of the volume f and the given C-arm images $p(\boldsymbol{\mu}'_j, f')$ is obtained when $\tilde{\boldsymbol{\mu}} = \boldsymbol{\mu}_0 \circ \boldsymbol{\mu}'$, where $\circ$ denotes a composition operator, and where $\boldsymbol{\mu}'$ is the arbitrary pose that we assigned when generating the given C-arm images.

4.2. Warping Index

To measure the precision of the estimation as a geometric error, we proceed as follows: using the known poses $\boldsymbol{\mu}_0 \circ \boldsymbol{\mu}'_j$, $j \in [1 \ldots N_p]$, we first project some arbitrary point of coordinate $\mathbf{x}$ onto the simulated C-arm images where it yields a set $K = \{\mathbf{k}_j\}$ of N_p coordinates $\mathbf{k}_j$. Then, using the (perhaps non-ideal) estimated parameters $\tilde{\boldsymbol{\mu}}_j$, we retroproject the set K. Each element $\mathbf{k}_j$ corresponds to a retroprojected line in space; by ensuring that the *relative* orientation of the simulated C-arms does not change during optimization, we also ensure that the intersection $\mathbf{y}(\mathbf{x}; \boldsymbol{\mu}_0 \circ \boldsymbol{\mu}', \tilde{\boldsymbol{\mu}})$ of the 3D lines does exist and is uniquely defined. Then, by scanning all coordinates $\mathbf{x}$ within the CT volume, we compute the average geometric error as

$$\varpi = \frac{1}{\mathrm{card}(f)} \sum_{\mathbf{x} \in f} \|\mathbf{x} - \mathbf{y}(\mathbf{x}; \boldsymbol{\mu}_0 \circ \boldsymbol{\mu}', \tilde{\boldsymbol{\mu}})\|.$$

4.3. Results

We performed our experiments on a brain CT volume of size $32 \times 32 \times 32$ voxels at the full resolution (volume f). We used $N_p = 2$ projections of size 100×100 pixels, and we set the corresponding projection planes to be perpendicular to each other. We run the registration 100 times. For each registration, we generated a random initial value for the parameters $\tilde{\boldsymbol{\mu}}$ as a disturbance around the parameters $(\boldsymbol{\mu}_0 \circ \boldsymbol{\mu}')$.

The rigid-body geometric transformation $\mathbf{g}_0$ applied to f to get f' corresponds to 1.2, 1.3, and 1.4 pixels of translation along the x-, y-, and z-axes, respectively. In addition, we performed a rotation of about 6.6 degrees

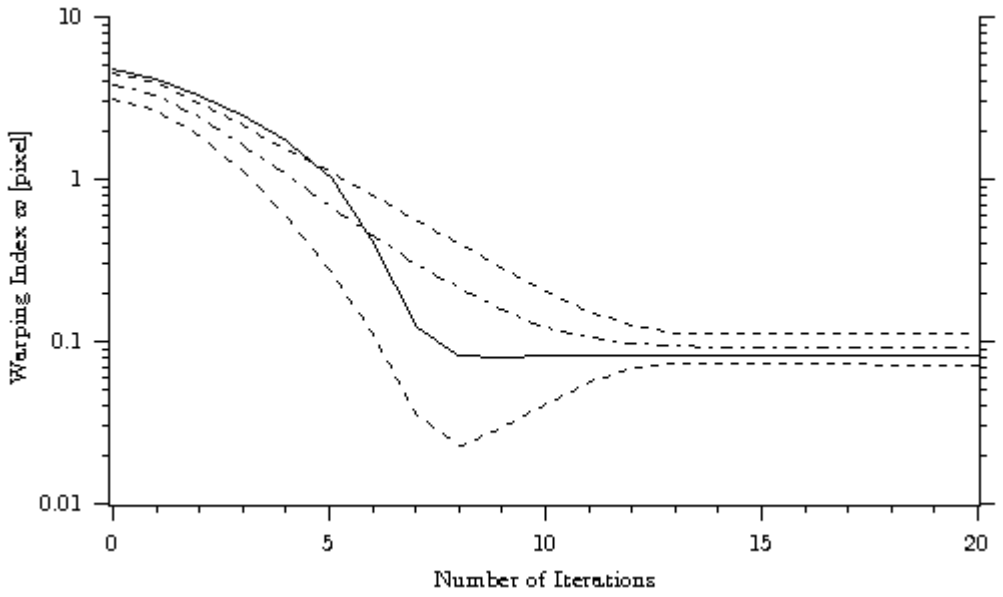

Figure 3. Performance of the registration algorithm for 100 randomly generated disturbances around the optimum solution. Solid line: Typical warping index *vs* number of iterations. Dash-dotted line: Average warping index. Dashed lines: Average $\pm\frac{1}{2}$ standard deviation of the warping index.

around a line through the volume center. The given C-arm images were obtained by projective integration of the volume f'. The pose of a given C-arm image $\boldsymbol{\mu}'$, that defines the pose of another given projection, was determined by a translation $\boldsymbol{\delta} = (10, 5, 7)$ pixels, and a rotation of about 93 degrees.

The simulated C-arm images were computed during the registration using the projective integration of the volume f. The initial parameters $\tilde{\boldsymbol{\mu}}$ were chosen as consisting in part of a normally-distributed translation with mean $\overline{\boldsymbol{\delta}} = (10, 5, 7)$ pixels and standard deviation $\sigma = 1.8$ pixels, and in part of a random rotation with mean 93 degrees and standard deviation 2 degrees. The warping index was computed over 40 iterations in each case.

Figure 3 shows a typical behavior of the warping index (solid line) on a linear-log scale. Starting from a large initial geometrical error (the initial warping index was approximately equal to 4.8 pixels), the algorithm succeeds to register the two images with a final geometrical error of approximately 0.08 pixels. Between the first and the third iteration, the gradient algorithm dominates so that the warping index decreases slowly from iteration to iteration, by less than 25 percents. From the fourth iteration, the Newton algorithm dominates so that the amelioration of the fit accelerates, the warping index decreases by more than 50 percents per iteration. After the ninth iteration, we observe that the algorithm has converged.

The algorithm was successful and resulted in a registration with a subpixel geometrical error in every case. Starting from a large initial geometrical error, the algorithm registered the two images in at most 14 iterations. At convergence, the mean and standard deviation of the warping index was 0.09 and 0.04 pixels, respectively. This residual misalignment is a consequence of the transformation $\mathbf{g}_0$ which was introduced to make the registration task more challenging.

5. DISCUSSION

We have proposed an algorithm for the accurate voxel-based 3D/2D registration of a preoperative CT volume with respect to intraoperative C-arm images. It takes advantage of a continuous image model made of cubic B-splines to accurately compute a series of simulated C-arm images for their comparison with the given C-arm images, along with the gradients needed for the optimization. The registration is accelerated by a method called projective integration that benefits from performing interpolation in 2D instead of 3D.

We have validated our algorithm in a controlled simulation environment where the true alignment is known *a priori*. This makes possible an objective evaluation of the quality of the registration. The algorithm was successful for each one of the 100 tests we performed and resulted in a subpixel performance of about a tenth of a pixel.

In the future, we plan to extend these results by evaluating our algorithm with true C-arm images. Moreover, we will integrate the present algorithm into a multiresolution approach, which should enhance speed and robustness.

Different multiresolution schemes have been applied for 3D/2D registration purposes. For example, Penney et al.[14] were using fluoroscopy images of a spine phantom reduced by blurring in order to register them with the CT image of the phantom; at each resolution level, the reduced fluoroscopy images were compared with the reduced 2D projections of the CT volume.

Two multiresolution strategies can be considered. The first one is based on computing a 3D pyramid for the CT volume on one hand, and a series of 2D pyramids for each of the given C-arm images on the other hand. During optimization, the simulated C-arm images would be projected from the relevant level of the CT pyramid. The other approach is to keep the full CT and to compute pyramids only for the given C-arm images. During optimization, every simulated projection would be first computed at full scale before to be reduced to the relevant resolution level. We expect the first approach to be faster but less accurate than the second one. Both approaches will be explored in our future work.

ACKNOWLEDGMENTS

This work was supported in part by grant Nb 2001-U13 from the AO ASIF Foundation, Switzerland.

REFERENCES

1. E. Bainville, I. Bricault, P. Cinquin, and S. Lavallée, "Concepts and methods of registration for computer-integrated surgery," in *Computer Assisted Orthopedic Surgery (CAOS)*, L. Nolte and R. Ganz, eds., pp. 15–34, Hogrefe & Huber Publishers, Seattle-Toronto-Bern-Göttingen, 1999.
2. L.-P. Nolte, M. Slomczykowski, U. Berlemann, M. Strauss, R. Hofstetter, D. Schlenzka, T. Laine, and T. Lund, "A new approach to computer-aided spine surgery: Fluoroscopy-based surgical navigation," *Eur. Spine J.* **9**, pp. 78–88, 2000.
3. M. Unser, A. Aldroubi, and M. Eden, "B-spline signal processing: Part I—Theory," *IEEE Trans. Signal Processing* **41**, pp. 821–832, 1993.
4. M. Unser, A. Aldroubi, and M. Eden, "B-spline signal processing: Part II—Efficient design and applications," *IEEE Trans. Signal Processing* **41**, pp. 834–848, 1993.
5. M. Unser, "Splines: A perfect fit for signal and image processing," *IEEE Signal Processing Magazine* **16**, pp. 22–38, 1999.
6. M. Unser, A. Aldroubi, and M. Eden, "The L_2 polynomial spline pyramid," *IEEE Trans. Pattern Anal. Machine Intell.* **15**, pp. 364–379, 1993.
7. P. Brigger, F. Müller, K. Illgner, and M. Unser, "Centered pyramids," *IEEE Trans. Image Processing* **8**, pp. 1254–1264, 1999.
8. S. Lavallée and R. Szeliski, "Recovering the position and orientation of free-form objects from image contours using 3-D distance maps," *IEEE Trans. Pattern. Anal. Machine Intell.* **17**, pp. 378–390, 1995.
9. A. Hamadeh, P. Sautot, S. Lavallée, and P. Cinquin, "Towards automatic registration between CT and X-Ray images: Cooperation between 3D/2D registration and 2D edge detection," in *Proc. MRCAS'95*, pp. 39–46, 1995.
10. A. Guéziec, P. Kazanzides, B. Williamson, and R. Taylor, "Anatomy-based registration of CT-scan and intra-operative X-Ray images for guiding a surgical robot," *IEEE Trans. Med. Imaging* **17**, pp. 715–728, 1998.
11. L. Lemieux, R. Jagoe, D. Fish, N. Kitchen, and D. Thomas, "A patient-to-computed-tomography image registration method based on digitally reconstructed radiographs," *Med. Phys.* **21**, pp. 1749–1760, 1994.
12. L. G. Brown and T. Boult, "Registration of planar film radiographs with computed tomography," in *IEEE Proc. MMBIA'96*, pp. 42–51, 1996.
13. J. Weese, G. Penney, P. Desmedt, T. Buzug, D. Hill, and D. Hawkes, "Voxel-based 2-D/3-D registration of fluoroscopy images and CT scans for image-guided surgery," *IEEE Trans. Inform. Technol. Biomedicine* **1**, pp. 284–293, 1997.

14. G. Penney, J. Weese, J. Little, P. Desmedt, D. Hill, and D. Hawkes, "A comparison of similarity measures for use in 2D-3D medical image registration," *IEEE Trans. Med. Imaging* **17**, pp. 586–595, 1998.
15. J. Weese, R. Gőcke, G. Penney, P. Desmedt, T. Buzug, and H. Schumann, "Fast voxel-based 2D/3D registration algorithm using a volume rendering method based on the shear-warp factorization," *Proc. SPIE'99 Image Processing* **3661**, pp. 802–810, 1999.
16. D. Marquardt, "An algorithm for least-squares estimation of nonlinear parameters," *J. Soc. Indust. Appl. Math.* **11**, pp. 431–441, 1963.
17. W. Press, B. Flannery, S. Teukolsky, and W. Vetterling, *Numerical Recipes*, The Art of Scientific Computing, Cambridge University Press, 1988.